Available online at www.sciencedirect.com
SCIENCE DIRECT®
Applied Catalysis A: General 260 (2004) 237–247
APPLIED CATALYSIS A: GENERAL
www.elsevier.com/locate/apcata

CoMo catalysts supported on aluminosilicates: synergy between support and sodium effects

V. La Parola [a,1], G. Deganello [a,b], A.M. Venezia [b,*]

[a] *Dipartimento di Chimica Inorganica e Chimica Analitica, S. Cannizzaro, Università di Palermo, Viale delle Scienze, Parco D'Orleans, 90128 Palermo, Italy*
[b] *Istituto per lo Studio dei Materiali Nanostrutturati, ISMN-CNR Sezione di Palermo, via Ugo La Malfa 153, 90146 Palermo Italy*

Received 22 July 2003; accepted 21 October 2003

Abstract

The structural properties and the hydrodesulfurization (HDS) activity of sodium doped and sodium free CoMo catalysts supported on amorphous aluminosilicates (ASA) were investigated as a function of different SiO_2:Al_2O_3 ratios. The support yielding the most active catalyst, (66% alumina) doped with different amounts of sodium, was used for a series of similar catalysts in order to study the effect of the alkali ion on the catalytic performance. The supports were prepared by sol–gel method and the catalysts were prepared by incipient wet impregnation method. The structure and the surface of the various samples were investigated by X-ray diffraction (XRD), temperature-programmed reduction (TPR) and X-ray photoelectron spectroscopy (XPS). The catalytic behaviour was tested in the hydrodesulfurization of thiophene carried out in a continuous flow system at atmospheric pressure, in a range of temperature between 603 and 633 K. Changes of activity with the support composition were observed. The presence of sodium, modifying the Brønsted acidity of the supports, enhances such effect. Moreover, the increase of the activity with increasing amount of sodium was a clear indication of the promoting effect of the alkali ion.

Keywords: Co-Mo catalysts; Sol–gel aluminosilicates; Silica/alumina ratio; HDS of thiophene; Sodium effect; XRD; XPS; TPR

1. Introduction

Hydrodesulfurization (HDS) processes consisting in the catalytic removal of sulphur from refinery stream is one of the most important processes in the modern refinery industrial plants [1,2]. Environmental restrictions regarding the quality of the transportation fuels impose to reduce sulphur content down to 30–50 ppm by 1 January 2005 [2]. New technologies based on dual stage processes and advanced reactor design to remove the least reactive sulphur compounds are being developed [3]. However, the interest in improving the traditional HDS catalysts based on cobalt promoted molybdenum sulphide supported on alumina or silica is still high. These catalysts are characterised by a low hydrogenation activity which results in relatively little consumption of hydrogen [2]. This property makes them attractive in the HDS of unsaturated hydrocarbon streams like FCC naphta. However, the conventional CoMo catalysts would allow to reach the imposed sulphur limit only by using severe hydrotreating conditions, like high pressure and high temperature, at the expenses of other fuel requirements, such as overall aromatics content, boiling range and olefin content for gasoline, and cetane number, density, polynuclear aromatics contents for diesel fuels [4,5]. Therefore, one of the important aims of the current industrial research is to prepare CoMo catalysts with improved activity and selectivity. As shown in several studies, the catalytic activity of the CoMo sulphide catalyst is determined by the synergy between the Co and the Mo sulphides in the system [1,6]. It is established that the active species in these types of catalysts is represented by a particular Co–Mo–S structure in which cobalt decorates the edges of MoS_2 slabs [1]. According to literature, two types of Co–Mo–S structures may form; the single slab, called type I, interacting strongly with the support, and the multiple slabs, called type II, exhibiting weak interaction with the support and considered the

* Corresponding author. Tel.: +39-091-6809372; fax: +39-091-6809399.
E-mail address: anna@pa.ismn.cnr.it (A.M. Venezia).
[1] Submitted by VLP in partial fulfillment of the requirements for the Ph.D. degree, University of Palermo, 2002.

0926-860X/$ – see front matter © 2003 Elsevier B.V. All rights reserved.
doi:10.1016/j.apcata.2003.10.020

most active form [7]. Both, the support and the preparation method in the presence of particular ligands determine the type of Co–Mo–S structure [8–11]. The importance of the precursor mixed oxide, β-$CoMoO_4$, on the formation of the active sulphide (type II) is still under debate [12,13]. We have recently shown that the addition of sodium to an aluminosilicate support, up to a certain loading, increased the HDS activity of the supported CoMo catalysts and at the same time promoted the formation of the mixed oxides β-$CoMoO_4$ [14]. On the contrary, in the case of pure silica supported catalysts, formation of the mixed oxide was observed in the absence of sodium ions, whereas in the presence of sodium the transformation of polymolybdate surface clusters into monomeric Na_2MoO_4 units at the expenses of the $CoMoO_4$ species [15,16] occurred. The presence of sodium at any concentration was detrimental for the HDS activity of the silica supported CoMo catalysts [15]. Therefore, the role of sodium on the HDS activity of the catalysts seemed to be related to the type of support. The observed modification of the catalyst structure, as evidenced by the formation of the $CoMoO_4$ in the ASA case and by the formation of the Na_2MoO_4 in the silica case, induced by sodium ions, may not be the only reason for the variation of the catalytic activity. Several studies had shown that the activity of amorphous aluminosilicates (ASA) used in acid catalysed reactions, strongly depend on the total amount of Brønsted and Lewis acid sites [17]. Moreover, both types of sites control the microstructure and also the chemical state of the supported Mo and Co oxides [18,19].

The opposite results on the effect of sodium on the HDS activity of the CoMo catalysts, obtained with the two different supports, commercial ASA and amorphous silica, prompted us with a more detailed study on the combination of the two effects; composition of the support in terms of Al/Si atomic ratio, affecting the surface acidity, and presence of sodium. To this purpose, supports with different Al/Si atomic ratio were prepared by sol–gel techniques [20,21] and used to make two series of supported CoMo catalysts with and without sodium. In order to investigate the effect of increasing amount of the alkali ion on the catalytic activity, a third series of catalysts on the support, yielding the most active catalyst (66% alumina), doped with different amounts of sodium, was prepared and investigated. Structural and surface characterisations of the catalysts and oxide precursors were obtained by X-ray diffraction (XRD), temperature-programmed reduction (TPR) and X-ray photoelectron spectroscopy (XPS).

2. Experimental

2.1. Supports and catalyst preparation

The aluminosilicate supports were prepared by sol–gel route according to the procedure described in [20]. All operations were performed under an atmosphere of pure argon. All chemicals (Aldrich) were of reagent grade purity and used as received. The required amounts of $Al(O\text{-}sec\text{-}Bu)_3$ and $Si(OEt)_4$ were mixed together. The solution was stirred 3 h at room temperature under Ar flow in order to obtain a homogeneous mixture. The temperature was then raised to 353 K and the hydrolysis was performed by adding water (pH 9 for ammonia) in stoichiometric amount to the rapidly stirred reaction mixture to allow the slow hydrolysis of the two alkoxides [22]. The gel, which formed in a few minutes, was left 5 h under reflux and constant stirring. Then it was aged in air inside the flask for 5 days at room temperature. The homogeneous and colourless gel was washed with sec-butanol to remove possible traces of unhydrolysed alkoxide. The washing fractions were completely clear on water addition. The xerogels were calcined in air at 773 K overnight. The list of prepared supports, s*x*, is given in Table 1. In the sample notation, *x* represents the ratio of the wt.% of alumina over silica. The series of supports doped with sodium was prepared by incipient wetness impregnation (WI) of the obtained supports with a solution of sodium nitrate, at the required concentration, then dried at 343 K for 2 h and then calcined in air at 773 K over night. Selected supports were analysed by IR spectroscopy of adsorbed pyridine in order to discriminate both Brønsted and Lewis acidity [20,23].

Table 1
Al/Si atomic ratios[a], wt.% alumina, surface areas (*S*) and zero point charges (ZPC) of the sol–gel prepared supports

Supports	Al/Si	Alumina (wt.%)	*S* ($m^2\ g^{-1}$)	ZPC
s∞	∞	100	210	9
s3	3.50	75	480	6.4
s2	2.34	66	488	5.6
	1.18	50	450	4.5
s0.3	0.39	25	355	4.1
s0.17	0.18	14.5	150	3.7
s0	0	0	143	5.2

[a] As obtained from fluorescence analyses [20].

The two series of catalysts, containing 7 wt.% Mo and 1.7 wt.% Co, on the pure aluminosilicates and on the sodium doped aluminosilicates, were prepared by incipient wetness impregnation, involving a first impregnation with aqueous solution of $(NH_4)_6Mo_7O_{24}{\cdot}4H_2O$ at pH 8, followed by 2 h drying at 343 K and overnight calcination at 773 K. Thereafter, the second impregnation with an aqueous solution of $Co(NO_3)_2{\cdot}6\ H_2O$ followed by the same steps as before was carried out [14]. The samples of the two series, without sodium and with 1 wt.% Na are labelled as s*x*WI and 1Nas*x*WI respectively. They are listed in Table 2 along with the corresponding surface areas. The support, s2, doped with different amounts of sodium, from 0.5 to 6 wt.%, was used for a third series of catalysts, labelled as *y*Nas2WI where *y* represents the wt.% of Na.

Table 2
Sodium free and sodium doped CoMo catalysts prepared by incipient wetness impregnation and after calcinations with the corresponding surface areas (S)

Sample	S ($m^2\,g^{-1}$)	Sample	S ($m^2\,g^{-1}$)
s∞WI	200	1Na s∞WI	230
s3WI	180	1Nas3WI	220
s2WI	290	1Nas2WI	232
s1WI	200	1Nas1WI	170
s03WI	170	1Nas03WI	110
s017WI	45	1Nas017WI	30
s0WI	85	1Nas0WI	80

2.2. Catalyst characterisation

2.2.1. X-ray diffraction

X-ray diffraction measurements for the structure determination were carried out with a Philips vertical goniometer using Ni-filtered Cu Kα radiation. A proportional counter and 0.05° step sizes in 2θ were used. The assignment of the various crystalline phases was based on the JPDS powder diffraction file cards [24].

2.2.2. BET analyses

The microstructural characterisation was performed with a Carlo Erba Sorptomat 1900 instrument. The fully computerised analysis of the adsorption isotherm of nitrogen at liquid nitrogen temperature, allowed obtaining, through the BET approach, the specific surface area of the samples. By analysis of the desorption curve, using the Dollimore and Heal calculation method, the pore size volume distribution was also obtained [25].

2.2.3. X-ray photoelectron spectroscopy (XPS)

The X-ray photoelectron spectroscopy analyses were performed with a VG Microtech ESCA 3000 Multilab, equipped with a dual Mg/Al anode. The spectra were excited by the unmonochromatised Al Kα source (1486.6 eV) run at 14 kV and 15 mA. The analyser operated in the constant analyser energy (CAE) mode. For the individual peak energy regions, a pass energy of 20 eV set across the hemispheres was used. Survey spectra were measured at 50 eV pass energy. The sample powders were analysed as pellets, mounted on a double-sided adhesive tape. The pressure in the analysis chamber was in the range of 10^{-6} Pa during data collection. The constant charging of the samples was removed by referencing all the energies to the C 1s set at 285.1 eV, arising from the adventitious carbon. The invariance of the peak shapes and widths at the beginning and at the end of the analyses ensured absence of differential charging. Analysis of the peaks were performed with the software provided by VG, based on non-linear least squares fitting program using a properly weighted sum of Lorentzian and Gaussian component curves after background subtraction according to Shirley [26] and Sherwood [27]. Constraints on the intensity ratios of the two Mo 3d and Co 2p doublet components were used in accord with the spin-orbit coupling rules. Atomic concentrations were calculated from peak intensity using the correction factors provided with the software. The binding energy values are quoted with a precision of ±0.15 eV and the atomic percentage with a precision of ±10%. Contact of the samples with air was minimised during sample loading; particular care was adopted for samples analysed after the HDS reaction.

2.2.4. Zero point charge determination (ZPC)

The ZPC of the various supports was determined by mass titration [20,28]. According to this method, the variation of pH of a water solution containing increasing amount of solid was monitored until the steady-state value of pH (ZPC) was reached.

2.2.5. Temperature-programmed reduction (TPR)

TPR measurements were conducted with a Micromeritics AutoChem 2910 Automated Catalyst Characterisation System, equipped with a thermal conductivity detector (TCD). About 0.1 g of sample was used for each measurement. The samples were pre-treated with a mixture of 5 vol.% O_2/He at 50 ml min^{-1} at 773 K for 30 min. After lowering the temperature down to 323 K, the gas mixture of 10 vol.% H_2/Ar was introduced at 10 ml min^{-1} into the sample loop and was also used as a reference gas. During the analysis, the temperature was increased to 1273 K at a rate of 10 K min^{-1}. The effluent gas was analysed with a thermal conductive detector.

2.3. HDS reaction

The hydrodesulfurization of thiophene was carried out in the vapour phase using a continuous flow microreactor and according to the procedure described previously [14,15]. An amount of 200 mg of catalyst (sieved fraction 210–430 μm), diluted with inert particles of SiC, was used for each test. The samples were sulphided in situ with a mixture of 10 vol.% H_2S/H_2, at 50 ml min^{-1}, while raising the temperature up to 673 K at a rate of 7 K min^{-1} and were maintained at this temperature for 2 h. After purging with nitrogen, the HDS of thiophene was carried out at 603 K with a mixture of 5.2 vol.% thiophene in H_2 at 25.7 ml min^{-1}. The absence of diffusion limitations was previously checked by observing the effect of the reactant flow rate on the conversion at constant space velocity (by simultaneously varying the flow and the bed depth). The reaction products were analysed by on-line gas chromatography (Carlo Erba GC 8340 gas chromatograph). Fractional conversions were calculated from the ratio of the peak area of the C_4 products over the sum of the peak areas of the products and thiophene. The pseudo first-order rate constant for HDS (k_{HDS}) was calculated by the equation: $k_{HDS} = -\ln(1-x)/\tau$, where x is the fractional conversion at the steady-state conditions, reached after 14 h on stream, and τ is the space time given by the mass of the catalysts (g) divided by the volumetric reagent

gas flow F_0 (ml s^{-1}). Conversions at the beginning of the reaction were also considered in order to determine the initial deactivation. For this purpose a percentage of deactivation defined as: $d = 100\%\cdot(x_i - x_f)/x_i$ with x_i and x_f being the conversion under initial and stationary conditions, was calculated. Measurements of the rate constants at different temperatures, allowed to determine the apparent activation energy for each catalyst [14]. Deactivation was checked by experiment of ascending and descending temperature. The relative error on the catalytic activity data was of the order of 10%.

3. Results

The properties of the supports in terms of surface areas and point of zero charge are listed in Table 1. Mixed oxides have generally higher surface areas as compared to the pure alumina or silica oxides. The PZC decreased from pure alumina toward the silica rich samples. The sol–gel prepared silica presented a rather high PZC as compared to literature values [20]. In accord with the previously reported pore distribution measurements, all the supports contain mesopores. The alumina rich samples have pores of size between 1 and10 nm, whereas the silica rich ones have pores of sizes between 10 and 30 nm [20]. In Fig. 1 the IR spectra of the adsorbed pyridine are shown for selected supports. The main features of the spectra are the stretching vibrations ν_{19b} band at 1455 cm^{-1} and the ν_{8a} band at 1620 cm^{-1} attributed to pyridine co-ordinated on Lewis sites [20]. The bands at 1540 cm^{-1} and at 1640 cm^{-1} are due to pyridinium ions formed on the Brønsted acid sites. The rather intense band at 1492 cm^{-1} is less informative, being associated with both the Brønsted and Lewis sites. With increasing the silica content the ratio of the Lewis/Brønsted sites decreases as s3 > s2 > s1 > s03. The resolution of the IR spectra did not allow to appreciate differences in the adsorption frequency attributable to different strength of the acid sites.

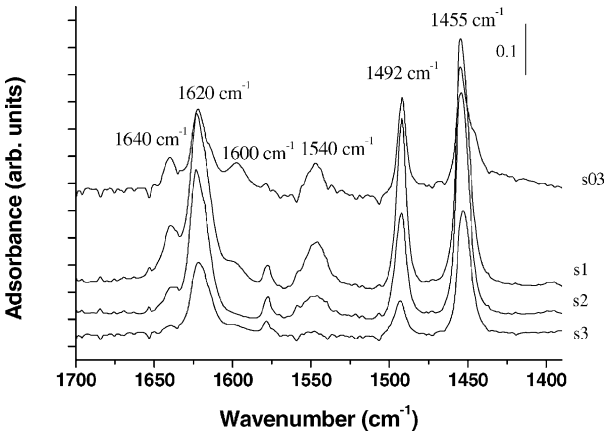

Fig. 1. FT-IR spectra of selected silica-alumina samples after admission of pyridine and subsequent outgassing at 423 K.

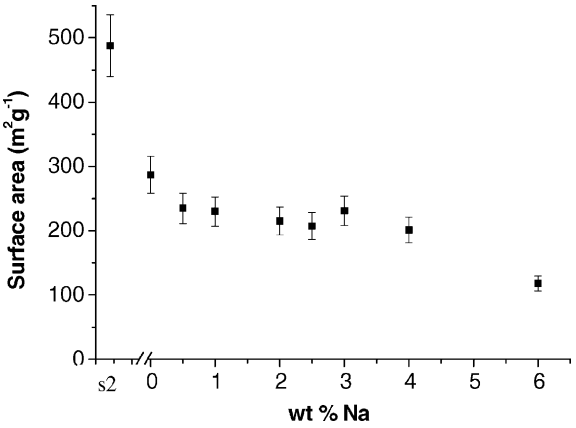

Fig. 2. Variation of the surface area as a function of the Na (wt.%) of the *y*Nas2WI catalysts. The area of the support, s2, is also given.

Moreover the IR spectra of the hydroxyl region was characteristic of silanol and bridged hydroxyl groups [20]. The addition of sodium to the supports determined a decreased of the Brønsted sites with respect to the Lewis sites [29].

As observed in Table 2, the surface areas of the supported Mo and Co catalysts are considerably lower than the areas of the corresponding supports. In the presence of 1 wt.% Na, no significant changes of the areas are found. The variation of the s2 supported catalyst area as a function of the amount of sodium is reported in Fig. 2. Beside the initial drop due to the addition of the supported metals, a substantial drop in surface area occurs for Na loading above 4 wt.%.

3.1. HDS activity

In Table 3, the catalytic activity results obtained with the sodium free and sodium doped catalysts are listed. The rate constants and deactivation percentages refer to the steady-state conditions at 603 K. The apparent activation energy was calculated in the range 603–633 K. The rate constants as a function of the different supports are shown in Fig. 3. A dependence of the activity from the Al_2O_3:SiO_2 ratio and the effect of the presence of 1 wt.% Na are clearly noticeable. The alumina rich catalysts are more active than the silica rich ones. In particular, the largest activity is found in correspondence of the s2 support containing 66% of alumina. A beneficial effect of sodium is observed in

Table 3
Catalytic activity results of catalysts without sodium and with 1 wt.% sodium

Sample	k (ml s^{-1} g^{-1})	d (%)	Sample	k (ml s^{-1} g^{-1})	d (%)
s∞WI	0.56	15	1Nas∞WI	0.36	15
s3WI	0.35	40	1Nas3WI	0.76	n.d.
s2WI	0.65	54	1Nas2WI	1.2	53
s1WI	0.27	73	1Nas1WI	0.54	66
s03WI	0.22	n.d.	1Nas03WI	0.18	68
s017WI	0.06	72	1Nas017WI	0.07	67
s0WI	0.15	62	1Nas0WI	0.023	n.d.

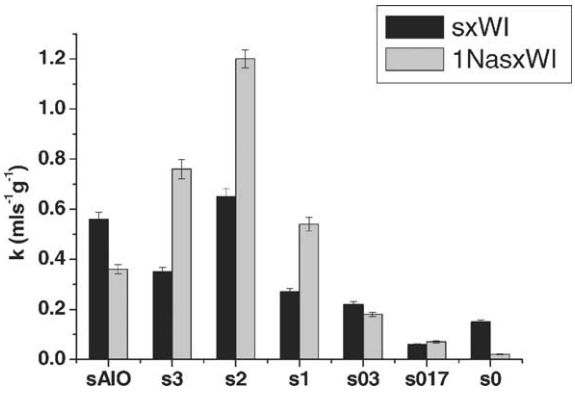

Fig. 3. Variation of the HDS rate constant with the support formulation for the sodium free and sodium doped series.

those catalysts with 75, 66 and 50 wt.%, of alumina in the supports. A detrimental effect of sodium occurs on the pure alumina, sA10 stands for s∞ pure silica and on the silica rich supported catalysts. As observed in Table 3, the initial deactivation percentage (*d*) occurs with any catalyst, however the deactivation is less with the pure alumina and increases in the ASA supported catalysts. This is in accord with the larger acidity of the ASA supports which favours formation of poisoning coke [30]. The presence of 1 wt.% sodium in the supports does not affect the initial deactivation. The apparent activation energy was obtained from the Arrhenius plot in the range 603–633 K. Above 633 K, deviation from the linearity occurred with all catalysts, with a distinct decrease of the activation energy at higher temperature [14]. This behaviour was previously explained with the decreased thiophene surface coverage at the increasing temperature [31]. An average activation energy of 57 kJ mol^{-1} has been measured for the sodium—free samples and a slight smaller value of 50 kJ mol^{-1} for the sodium doped samples. The catalytic activity of the *y*Nas2WI series is shown in Fig. 4 where the rate constants versus the wt.% Na are reported. A distinctly positive effect of the alkali

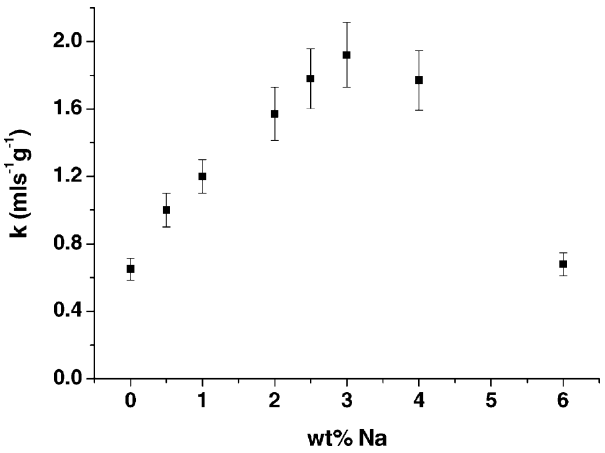

Fig. 4. Variation of the rate constant, *k*, versus Na (wt.%) for the s2 supported catalysts, *x*Nas2WI.

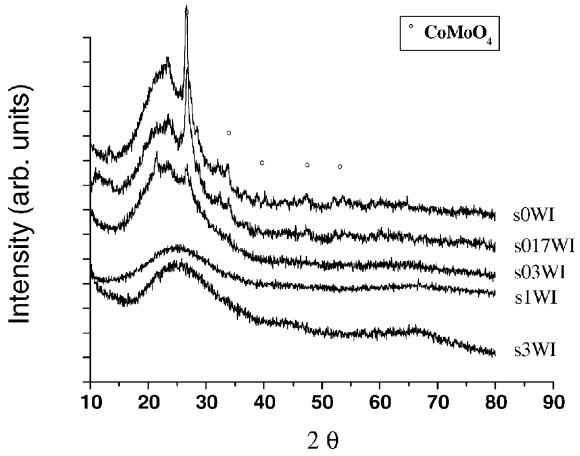

Fig. 5. X-ray diffractograms of the calcined sodium-free catalysts.

ions is observed, with a three times increase of the activity in correspondence of 3 wt.% of sodium.

3.2. Catalyst characterisation

3.2.1. X-ray diffraction

The X-ray diffractograms of the sodium—free samples are shown in Fig. 5. Same patterns were obtained with the corresponding 1 wt.% sodium doped samples. The pure alumina supported catalyst, not shown in the figure, exhibited the γ-alumina pattern of the support. The alumina rich samples exhibited the amorphous patterns typical of the corresponding supports [20]. With increasing silica content (from s03 to s0), peaks of the β-$CoMoO_4$ [24] of increasing intensity appeared. The results are in accord with literature, where the formation of such phase is reported to occur on silica, for calcination temperature close to those used in the present study, and on alumina for temperature above 873 K [32]. The appearance of diffraction lines attributed to Na_2MoO_4, in the sample with 6 wt.% Na is the only structural variation observed within the *y*Nas2WI catalyst series.

3.2.2. Temperature-programmed reduction

The interaction between the metals and the support in the oxidic form of the catalysts was investigated by TPR. The obtained TPR profiles are shown in Fig. 6. The hydrogen consumption and the characteristic T_m (temperature at maximum) are listed in Table 4. In order to evaluate synergetic effects between the two metals, the monometallic Cos2WI and Mos2WI catalysts, supported on s2 and with the same metal loading of the bimetallic catalysts, were prepared and analysed by TPR. The data from the corresponding TPR profiles, shown in Fig. 7, are also reported in Table 4. The consumption of hydrogen is much larger for the Mos2WI sample than for the Cos2WI sample. Moreover the close similarity of the two profiles, the one relative to the bimetallic s2WI and the one relative to the monometallic Mos2WI, suggests that, at the used metal loading, the contribution of the cobalt to the hydrogen consumption profile is negligible.

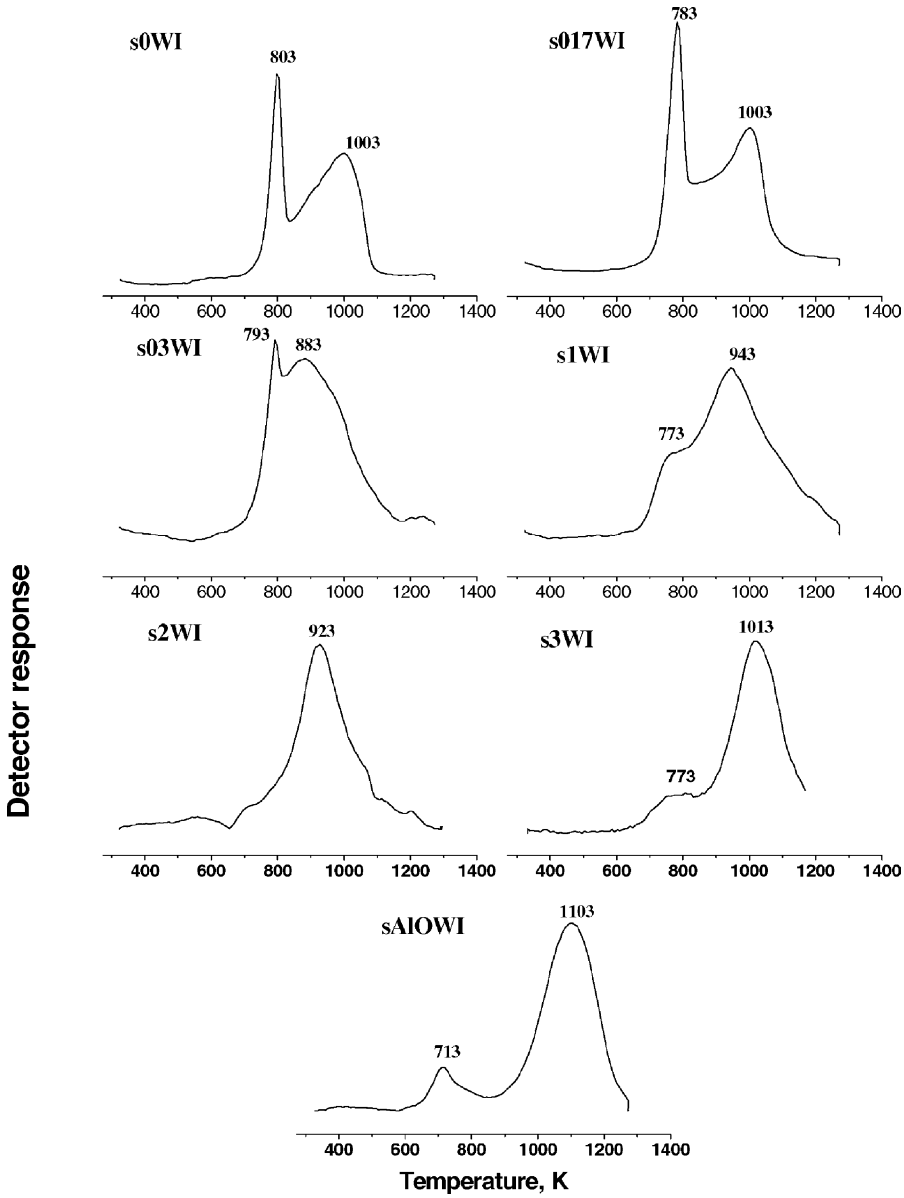

Fig. 6. TPR profiles of catalysts without sodium on different supports.

Table 4
TPR peaks (±15 K) and H_2 uptake (±15%) of the calcined catalysts, sxWI

Sample	T_1 (K)	V_1 (ml g^{-1})	T_2 (K)	V_2 (ml g^{-1})	($V_1 + V_2$) (ml g^{-1})
Mos2WI	–	–	953	23	23
Cos2WI	–	–	853	6	6
s∞WI	713	4	1103	29	33
s3WI	773	4	1013	22	26
s2WI	–	–	923	31	31
s1WI	773	4	943	20	24
s03WI	793	8	883	21	29
s017WI	783	13	1003	15	28
s0WI	803	11	1003	24	35

According to Fig. 6 and Table 4, the shape and the maxima of the catalyst profiles are strongly dependent on the support composition.

The catalyst on pure silica and the one on pure alumina, s0WI and s∞WI, respectively, are characterised by two peaks. The low temperature peak, T_1, is attributed to the partial reduction of Mo^{6+} to Mo^{4+} of amorphous, highly defective, multilayered oxides (octahedral Mo species). The high temperature peak, T_2, is attributed to the deep reduction of all Mo species, including highly dispersed monomeric tetrahedral Mo(VI), which are mostly stabilised on the surface of the alumina support [33–35]. In all cases, the hydrogen consumption relative to T_2 is quite larger than that of T_1.

In the pure alumina catalyst, where the interaction between the Mo and the support is stronger than in the silica

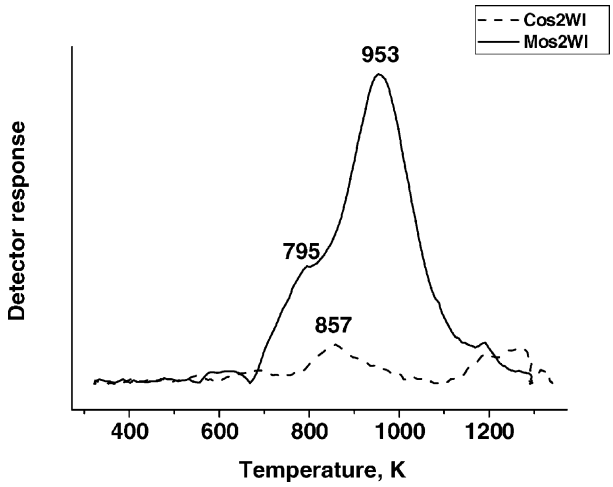

Fig. 7. TPR profiles of Mos2WI e Cos2WI.

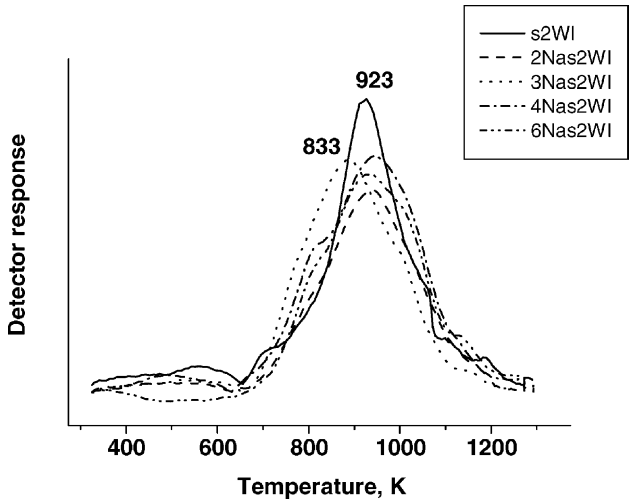

Fig. 8. TPR profiles of *y*Nas2WI catalysts.

case, most of the reduction occurs at a higher temperature (main peak at 1103 K) and involves the deep reduction, from Mo^{6+} to Mo^{0}. The partial reduction of traces of polymolybdate species aggregates gives rise to the small low temperature peak at 713 K.

In the pure silica catalyst, the two-step reduction process is more evident. In accord with the hydrogen consumption values, the low temperature peak at 803 K refers to the first reduction step, from Mo^{6+} to Mo^{4+}, whereas the high temperature peak at 1003 K refers to the second reduction step from Mo^{4+} to Mo^{0}.

The catalysts supported on the mixed oxides present features of both the pure alumina and pure silica supported catalysts. Overall, by increasing the alumina content, the hydrogen consumption of the low temperature peak decreases. The values of the total hydrogen consumption for all the catalysts are, within the experimental error, quite comparable, in accord with the same total metal concentration.

The TPR data of the 1 wt.% Na doped samples did not differ much from the corresponding sodium free sample data. As shown in Fig. 8, increasing amount of sodium in the s2 support changed slightly the TPR profile of the s2WI sample. The main effect of sodium seems to be a broadening of the peak which, especially in the 3Nas2WI is found shifted to a low temperature.

3.2.3. XPS

The binding energies of the Mo $3d_{5/2}$, Co $2p_{3/2}$ with the relative atomic concentrations are listed in Table 5, for the pure silica and for the ASA supported catalysts in the oxidic state. In Table 6, the corresponding data are listed for the sodium containing catalysts. The Mo 3d spectra presented the two spin-orbit components, $3d_{5/2}$ and $3d_{3/2}$ with an energy separation of 3.1 eV [16]. No significant changes of the Mo 3d binding energy with the different support composition are found [36,37]. The Mo $3d_{5/2}$ binding energies are typical of Mo(VI) [16]. The broadness of the peaks is an indication of several Mo(VI) oxo-species [16,36]. The presence of 1 wt.% sodium does not affect the binding energies. However, especially in the silica rich samples, as already noticed [16] for silica supported catalysts, sodium determines a narrowing of the peaks, attributed to the sodium induced transformation of polymolybdates clusters into monomeric units.

Table 5
Mo $3d_{5/2}$, Co $2p_{3/2}$ binding energies and XPS derived Mo and Co atomic percentage of the calcined catalyst, s*x*WI

Sample	Mo $3d_{5/2}$ (eV)	Co $2p_{3/2}$ (eV)	Mo (at.%)	Co (at.%)
s3WI	233.0 (2.8)	781.1 (5.3)	1.2	1.3
s2WI	232.6 (2.8)	781.3 (3.8)	1.5	0.5
s1WI	232.9 (3.0)	781.8 (3.9)	1.4	0.5
s03WI	232.6 (3.2)	782.2 (4.7)	0.7	0.8
s0WI	232.9 (2.5)	n.d.	0.5	n.d.

The full widths half maximum are given in parentheses.

Co 2p spectra, shown in Fig. 9, are characterised by the two spin-orbit components and by the presence of strong shake up satellites typical of high spin Co(II) species. As compared to the molybdenum case, the Co 2p spectra are more affected by the different supports in terms of signal intensity and binding energy position. As shown in Table 5, the Co $2p_{3/2}$ binding energy of the sodium-free samples shifts towards lower value along the series from the silica rich to the pure alumina samples. As indicated in Table 6, the

Table 6
Mo $3d_{5/2}$, Co $2p_{3/2}$ binding energies and XPS derived Mo and Co atomic percentage of the calcined catalysts, 1Nas*x*WI

Sample	Mo $3d_{5/2}$ (eV)	Co $2p_{3/2}$ (eV)	Mo (at.%)	Co (at.%)
1Nas3WI	232.7 (2.7)	781.5 (3.8)	0.9	1.0
1Nas2WI	232.6 (2.7)	781.0 (4.3)	1.3	0.6
1Nas1WI	233.0 (2.8)	781.7 (4.2)	1.6	0.8
1Nas03WI	232.6 (2.5)	781.0 (4.3)	1.3	1.0
1Nas0WI	232.3 (2.5)	n.d.	0.4	n.d.

The full widths at half maximum are given in parentheses.

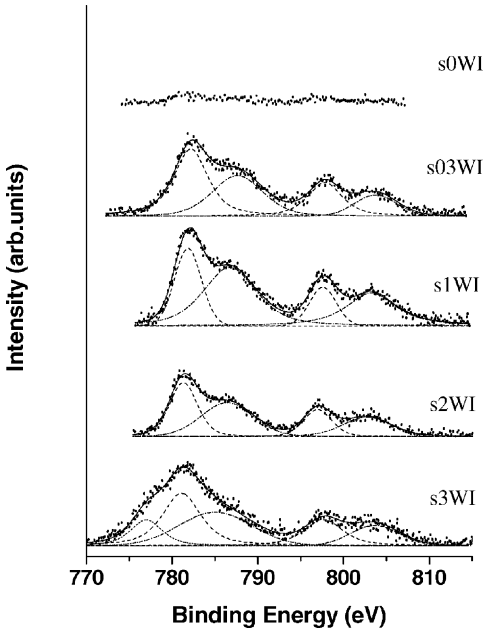

Fig. 9. Co 2p photoelectron spectra of the sodium free catalysts.

presence of sodium removes such effect and rather similar Co binding energy values are obtained for the catalysts on the different supports. The extra peak fitted at 777.3 eV, in the Co 2p region of the s3WI catalyst, shown in Fig. 9, is attributed to a Co Auger LMM transition, rather than to a reduced cobalt species [38].

Concerning the distribution of Mo and Co at the catalyst surface, as observed from the XPS derived atomic percentages listed in Table 5, all the catalysts are surface enriched in Mo and Co with respect to the analytical contents. By increasing the amount of silica in the support, both Mo and Co surface atomic concentrations decrease. This effect is larger for the cobalt which, as shown in Fig. 9, is completely undetected in the pure silica supported sample. The presence of 1 wt.% of sodium in the supports has little effect on the surface atomic concentration of Co and Mo. However, as shown by the results of the XPS investigation of the *y*Nas2WI series, summarised in Table 7, increasing amount of sodium determines a surface enhancement of the cobalt species. The surface sodium concentrations, in good agreement with the sodium nominal loadings, indicate a rather uniform distribution of sodium through the samples.

Table 7
Mo $3d_{5/2}$, Co $2p_{3/2}$ binding energies and XPS derived Mo, Co and Na atomic percentage of the calcined catalysts, *y*Nas2WI

Sample	Mo $3d_{5/2}$	Co $2p_{3/2}$	Mo (at.%)	Co (at.%)	Na (at.%)
s2WI	232.6 (2.8)	781.3 (3.8)	1.5	0.5	–
0.5Nas2WI	232.4 (2.8)	780.9 (3.2)	1.4	0.7	0.5
1Nas2WI	232.6 (2.7)	781.0 (4.3)	1.3	0.6	1.4
2Nas2WI	232.7 (2.5)	781.2 (3.3)	1.2	0.7	2.0
2.5Nas2WI	232.7 (2.3)	781.2 (3.0)	1.3	0.7	3.2
3Nas3WI	232.6 (2.5)	781.2 (3.3)	1.3	0.6	3.3
4Nas2WI	232.4 (2.4)	780.6 (3.3)	1.5	1.5	4.3
6Nas3WI	232.6 (2.3)	780.6 (3.3)	1.6	1.7	7.8

The full widths at half maximum are given in parentheses.

Selected catalysts have been analysed by XPS after being used in the catalytic reaction. The Mo 3d spectra and the Co 2p spectra of the selected samples s2WI and 1Nas2WI before and after the HDS reaction are shown in Figs. 10 and 11, respectively. The corresponding binding energies are listed in Table 8. Concerning the Mo 3d spectral region, the spectra of the aged samples contain the peak of the S 2s at 225.6 eV [15] and three Mo 3d doublets. The Mo $3d_{5/2}$ at the highest energy, at ≈232 eV, is attributed to unreduced Mo(VI). The Mo $3d_{5/2}$ at ≈230 eV is indicative of an intermediate oxidation state which is not clearly identified. According

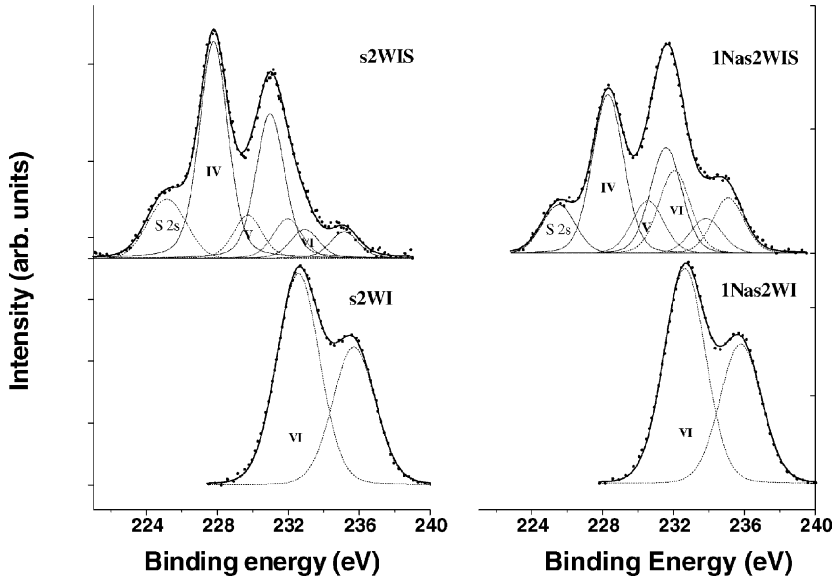

Fig. 10. Mo 3d and S 2s photoelectron spectra of fresh and aged s2WI and 1Nas2WI samples.

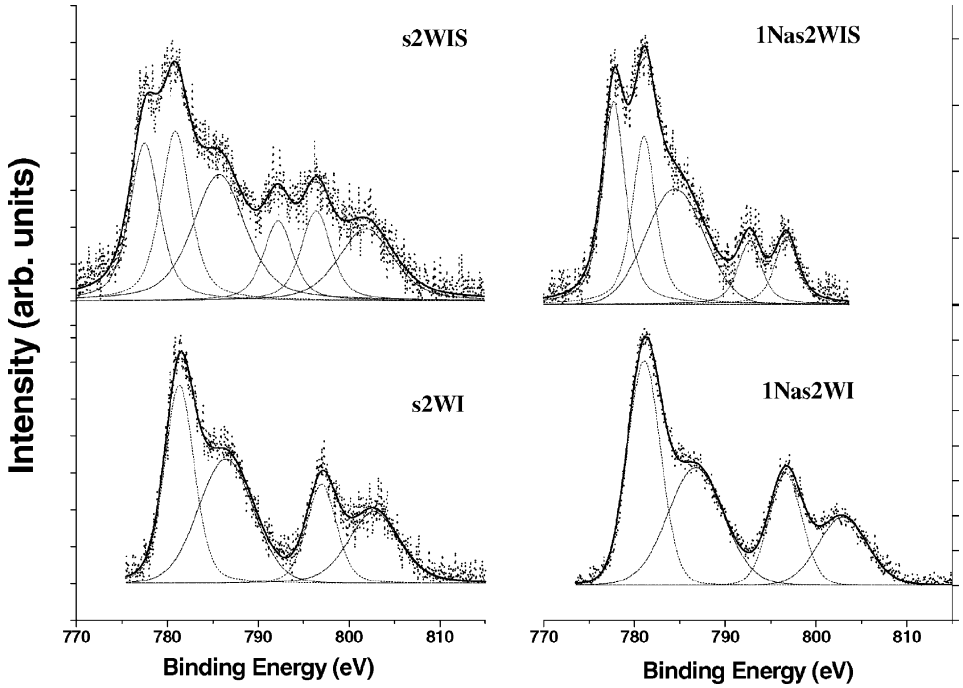

Fig. 11. Co 2p photoelectron spectra of fresh and aged s2WI and 1Nas2WI samples.

to literature it could be due to Mo(V) [39]. The presence of mixed oxy-sulphide, –S–Mo^{6+}–O– can not be excluded. The sulfurisation at low temperature may proceed through an exchange between oxygen and sulphur. The replacement of the oxygen atoms by the less negative sulphur atoms, may determine a decrease of the Mo(VI) binding energy [40,41]. This would explain also the small decrease of the binding energy value of the high energy peak of the samples after HDS (compare corresponding values of Tables 8 and 5). The peak at ≈228 eV is attributed to the reduced Mo(IV) as oxide or as sulphide [15]. It is worth noticing that the FWHM of the Mo 3d components decreases after reaction.

Table 8
Mo $3d_{5/2}$, Co $2p_{3/2}$ binding energies and atomic ratio of S over Mo(IV) of selected aged catalysts

	Mo $3d_{5/2}$ (eV) (%)	Co $2p_{1/2}$ (eV) (%)	S/Mo(IV)
s2WIS	227.8 (1.9) (72) 229.7 (15) 231.9 (13)	777.5 (3.5) (30) 780.9 (70)	2.2 ± 0.2
1Nas2WIS	228.3 (2.0) (54) 230.5 (16) 231.9 (30)	777.7 (2.8) (40) 781.0 (60)	2.2 ± 0.1
s0WIS	228.3 (1.8) (67) 230.4 (12) 232.2 (21)	n.d.	1.9 ± 0.2
1Nas0WIS	228.2 (1.9) (66) 230.0 (16) 232.0 (18)	n.d.	2.1 ± 0.2

The full widths at half maximum (eV) and the relative percentage of the components are given in parentheses.

As shown from Table 8, the cobalt spectra of the s2 supported samples after reaction exhibit the Co(II) component at ≈781 eV and a component at 777.6 eV attributable to Co(0) or to Co_9S_8 [42,43]. Similarly to the unused catalysts, the samples on pure silica, s0, with and without sodium did not give any appreciable Co 2p signal. The atomic ratios, S/Mo(IV), given in the table are in accord with the formation of stoichiometric MoS_2 and confirm the attribution of the low energy Co $2p_{3/2}$ peak to a Co(0) species rather than to Co_9S_8. According to the data no significant differences are found between the catalysts on the two different supports and with or without sodium.

The XPS analysis of the aged *y*Nas2WI series confirmed the above results. Mo was present as Mo(VI), Mo(V) and Mo(IV) and Co as Co(II) and Co(0).

4. Discussion

The catalytic results on the hydrodesulfurization of thiophene, showed a dependence of the HDS activity on the support composition in terms of silica/alumina ratio. A maximum of activity in correspondence of the s2 support and, thereafter, a decrease of activity with the increasing of the silica content was found. Such dependence was modulated or differently influenced by the presence of 1 wt.% Na in the supports. The support composition affected also the phase of the supported elements in the oxidic state. Indeed on silica and silica rich samples, from s0 up to s03, the $CoMoO_4$ phase was detected, at variance with the alumina rich samples showing only the amorphous structure of the original supports. Differences in the support surface area and poros-

ity did not correlate with the activity, suggesting that morphology was not relevant for the catalytic activity. Through the investigation of the support surface acidity by IR, a decreasing ratio of Brønsted/Lewis acid sites with the decreasing silica content was determined. These acid sites may be responsible for the dispersion and electronic effects of the active metals. Generally, alumina, exhibiting some Lewis acid sites, has a strong interaction with the metals. Such interaction is positive from the point of view of the good oxide dispersion but may be detrimental for the reducibility and therefore sulphidability of the Mo and Co oxides and it is believed to give rise to the less active phase Co–Mo–S(I) [8,44]. On pure silica, presenting only Brønsted acid sites, the interactions are weaker and the metal, freer to move on the support, may easily sinter [37]. Indeed, XPS analysis has evidenced a much lower surface concentration of the active elements in the pure silica and in the silica rich samples. As shown in Fig. 9, in the pure silica, cobalt was not detected at all. Moreover, the lack of any detectable crystalline phases, in the X-ray diffractograms of the alumina and alumina rich samples, could also be a sign of a better surface dispersion of the active metals.

The most direct measurement of the metal-support interaction is given by the TPR profiles of the calcined catalysts. According to the temperature of the peak maxima, the mixed oxide catalysts present an intermediate metal-support interaction with respect to the pure silica and pure alumina catalysts. Moreover, the TPR profiles can also be explained on the basis of the polarizability of the Mo–O–X bond with X = Al or Si. The Al strongly polarises the bond, making it more difficult to reduce. Some of the Mo–O–X links which remain in the sulphided catalysts, as proved by the Mo 3d photoelectron spectra of the aged samples, can polarise the Mo–S link [45]. According to Harris and Chianelli, the more ionic is the Mo–S bond the less active is the metal sulphide [46]. The increasing amount of silica in the mixed oxides causes an overall decrease of the polarizability of the Mo–O–X bond and, by increasing the covalency of the Mo–S bonds, increases the HDS activity. According to this view, the strength of the Mo–O–X links has a crucial role: it determines a better dispersion of the active species, but may produce more ionic Mo–S bond which are believed to be less HDS active. The number and the polarizability of the Mo–O–X links can be related to the type of surface acidity of the support. Since terminal Brønsted sites (like silanols in pure silica) are weaker acid sites as compared to the Lewis sites or to the bridged hydroxyl, they give rise to weaker metal-support interaction, and therefore to a worse dispersion and to a decreased polarizability. The enhanced activity found for the catalyst supported on s2 may be reasonably attributed to the particular combination of Brønsted/Lewis acidity of the support.

The effect of sodium on the catalytic behaviour depended on the type of support. In the pure oxides, the presence of sodium was detrimental, whereas in the mixed oxides, specially the alumina rich ones, the effect was definitely positive. From the structural point of view, beside an increase of the cobalt dispersion, observed in the oxidic catalysts, the presence of sodium determined a decrease of the Brønsted/Lewis acid site ratio of the supports [47]. The reduced number of Brønsted sites in the mixed oxide supports would drive, during the impregnation stage, the active metals towards the more interacting and more polarising Lewis sites. However, these sites are less interacting and less polarisable in the mixed oxide supports as compared to the sites of the pure alumina, and therefore generate more reducible oxymolybdate species. The weakening of the metal-support interaction, induced by sodium, determines a slight variation of the TPR patterns. As shown for the series of catalysts supported on s2, the promoting effect of sodium on the activity increases with sodium content up to 3 wt.%, thereafter the effect decreases. For sodium loading of 6 wt.% the activity returns equal to the activity of the undoped s2WI catalyst.

The detrimental effect of sodium in the pure silica supported catalyst was already documented and attributed to structural effects such as the transformation of the more active polymolybdate species into the monomeric, Na_2MoO_4 species [15]. In the case of the pure alumina supported catalyst, sodium would neutralise the Brønsted sites and again drive the active species toward the Lewis sites which in this case would interact quite strongly with the metals producing a worse catalyst. These results confirm the positive effect of sodium previously found on an ASA supported CoMo catalysts [14], but most interestingly is the finding of a synergy between sodium and support acidity. Accordingly, by choosing the appropriate support acidity and playing with the amount of sodium, it could be possible, in principle, to improve the activity of the CoMo catalysts.

5. Conclusion

The results of this study can be summarised in the following statements. The hydrodesulfurization activity of the Co-Mo catalysts supported on sol–gel prepared aluminosilicates depends on the Al/Si atomic ratio. By changing the support composition, the ratio between the Brønsted and the Lewis acid sites is changed. On silica, where the Lewis sites are absent, the active metals are supported through the Brønsted sites giving rise to weak metal-support interaction determining a poor dispersion of the active species; on pure alumina, through the Lewis acid sites, stronger metal-support interactions are achieved, producing better dispersed active species, quite hard to reduce and therefore to sulphide. On the mixed oxide a good compromise between the two types of oxides affords Mo–O–X links which are better dispersed on the support surface as compared to the silica case, and which are more easily reduced during the sulphiding treatment with respect to the alumina case.

Sodium, by neutralising the Brønsted sites, drives the active elements towards the Lewis sites. The effect of the sodium is therefore different for each support and it depends

on the Brønsted/Lewis acid site ratio. In the case of pure silica and pure alumina, even through different mechanisms, sodium is detrimental for the HDS activity of the supported catalysts. In the case of the mixed oxides, the favoured interactions between the metals and the less interacting Lewis acid sites is beneficial since produce better dispersed and more reducible oxidic species.

References

[1] H. Topsøe, B.S. Clausen, F.E. Massoth, Hydrotreating Catalysis, in: J.R. Anderson, M. Boudart (Eds.), Springer-Verlag, Berlin, 1996.
[2] I.V. Babich, J.A. Moulijn, Fuel 82 (2003) 607.
[3] S.T. Sie, Fuel Process. Technol. 61 (1999) 1.
[4] S.F. Venner, Hydrocarbon Process 5 (2000) 51.
[5] U. Hattiangadi, M. Spoor, S.C. Pal, Petr. Tech. Quart. 4 (2000) 35.
[6] C. Wivel, R. Clausen, B.S. Clausen, S. Morup, H. Topsøe, J. Catal. 68 (1981) 783.
[7] R. Candia, O. Sørensen, J. Villadsen, N. Topsøe, B.S. Clausen, H. Topsøe, Bull. Chim. Belg. 93 (1984) 763.
[8] S.M.A.M. Bouwens, J.A.R. van Veen, D.C. Koninnngsberger, V.H.J. de Beer, R. Prins, J. Phys. Chem. 95 (1991) 123.
[9] M. Breysse, J.L. Portefaix, M. Vrinat, Catal. Today 10 (1991) 489.
[10] Y. Okamoto, K. Ochiai, M. Kawano, K. Kobayashi, T. Kubota, Appl. Catal. A 226 (2002) 115.
[11] J.A.R. van Veen, E. Gerkema, A.M. van der Kraan, A. Knoester, J. Chem. Soc. Chem. Commun. 1684 (1987).
[12] J.I. Brito, A.L. Barbosa, J. Catal. 171 (1997) 467.
[13] J.A.R. van Veen, E. Gerkema, A. M van der Kraan, P.A.J.M. Hendricks, H. Beens, J. Catal. 133 (1922) 122.
[14] A.M. Venezia, F. Raimondi, V. La Parola, G. Deganello, J. Catal. 194 (2000) 393.
[15] A.M. Venezia, V. La Parola, G. Deganello, D. Cauzzi, G. Leonardi, G. Predieri, Appl. Catal. A 229 (2002) 261.
[16] V. La Parola, G. Deganello, C.R. Tewell, A.M. Venezia, Appl. Catal. A 235 (2002) 171.
[17] P. Yarlagadda, C.R.F. Lund, E. Ruckenstein, J. Catal. 125 (1996) 421.
[18] S. Rajagopal, H.J. Marini, J.A. Marzari, R. Miranda, J. Catal. 147 (1994) 428.
[19] R.G. Leliveld, T.G. Ros, A.J. van Dillen, J.W. Geus, D.C. Koningsberger, J. Catal. 185 (1999) 513.
[20] V. La Parola, G. Deganello, S. Scirè, A.M. Venezia, Solid State Chem. 174 (2003) 482.
[21] J. Livage, M. Henry, C. Sanchez, Prog. Solid State Chem. 18 (1988) 259.
[22] J.B. Miller, I.E. Ko, Catal. Today 35 (1997) 269.
[23] H. Knozinger, Adv. Catal. 25 (1976) 185.
[24] JCPDS Powder Diffraction File International Centre for Diffraction Data, Swarthmore.
[25] S.J. Gregg, K.S. Sing, Adsorption, Surface Area and Porosity, second ed., Academic Press, San Diego, 1982.
[26] D.A. Shirley, Phys. Rev. B5 (1972) 4709.
[27] P.M.A. Sherwood, in: D. Briggs, M.P. Seah (Eds.), Practical Surface Analysis, Wiley, New York, 1990, p. 181.
[28] S. Subramanian, J.S. Noh, J.A. Schwarz, J. Catal. 114 (1988) 433.
[29] Z. Sarbak, Appl. Catal. A. 164 (1997) 13.
[30] E. Furimsky, F.E. Massoth, Catal. Today 52 (1999) 381.
[31] E.J.M. Hensen, M.J. Vissenberg, V.H.J. de Beer, J.A.R. van Veen, R.A. van Santen, J. Catal. 163 (1996) 429.
[32] Y. Okamoto, T. Imanaka, S. Teranishi, J. Catal. 65 (1980) 448.
[33] S. Rajagopal, H.J. Marini, J.A. Marzari, R. Miranda, J. Catal. 147 (1994) 417.
[34] L. Qu, W. Zhang, P.J. Kooyman, R. Prins, J. Catal. 215 (2003) 7.
[35] Y.V. Plyuto, I.V. Babich, I.V. Plyuto, A.D. Van Langeveld, J.A. Moulijn, Colloids Surf. A 125 (1997) 225.
[36] Y.V. Plyuto, I.V. Babich, I.V. Plyuto, A.D. Moulijn, J.A. Langeveld, Appl. Surf. Sci. 119 (1997) 11.
[37] C.V. Caceres, J.L.G. Fierro, J. Lazaro, A. Lopez Agudo, J. Sorja, J. Catal. 122 (1990) 113.
[38] J. Chastain (Ed.) Handbook of X-ray Photoelectron Spectroscopy, Perkin-Elmer, Eden Prairie, MN, 1992.
[39] J. Yasumaru, M. Yamada, M. Houalla, D.M. Hercules, Proceedings of 10th International Congress, Catal. B (1993)1867.
[40] P. Arnoldy, J.A.M. van den Heijakant, G.D. de Bok, J.A. Mouljin, J. Catal. 92 (1985) 35.
[41] P. Dufresne, N. Brahma, F. Labruyere, M. Lacroix, M. Breysse, Catal. Today 29 (1996) 35.
[42] R. Riva, H. Miessner, R. Del Piero, G. Vitali, Appl. Catal. A 196 (2000) 111.
[43] A. Galtayries, J. Grimblot, J. Electron Spectrosc. Relat. Phenom. 98 (1999) 267.
[44] L. Medici, R. Prins, J. Catal. 163 (1996) 28.
[45] B. Scheffer, P. Arnoldy, J.A. Moulijn, J. Catal. 112 (1988) 516.
[46] S. Harris, R.R. Chianelli, J Catal. 86 (1984) 400.
[47] P.O. Fritz, J.H. Lunsford, J. Catal. 118 (1989) 85.